Neuroendocrinology Letters Volume 46 No. 7 2025
ISSN: 0172-780X; ISSN-L: 0172-780X; Electronic/Online ISSN: 2354-4716
Web of Knowledge / Web of Science: Neuroendocrinol Lett
Pub Med / Medline: Neuro Endocrinol Lett

ORIGINAL ARTICLE

Cross-organ single-cell integration identifies liver-specific fibroblast programs and HGF–MET/AGT–AGTR1B axes that link fibrosis to hepatocarcinogenesis

Shuna Zhang[1], Pei Sun[2], Jian Zhang[2], Xin Li[1,2]

1 Department of Center of Infectious Disease, Peking University Ditan Teaching Hospital, No. 8, Jingshun East Street, Beijing 100015, China.
2 Department of Center of Infectious Disease, Beijing Ditan Hospital, Capital Medical University, No. 8 Jing Shun East Street, Beijing 100015, China .

Correspondence to: Xin Li
Department of Center of Infectious Disease, Peking University Ditan Teaching Hospital, No. 8, Jingshun East Street, Beijing 100015, China
tel.: +8613910908996; e-mail: leaxin@ccmu.edu.cn;
orcid: https://orcid.org/0000-0002-2460-8753

Submitted: 2025-11-20 Accepted: 2025-12-24 Published online: 2025-12-29

Key words: **Single-cell integration; Liver fibrosis; Cross organ; Hepatocyte–fibroblast communication; Hepatocellular carcinoma**

Neuroendocrinol Lett 2025; **46**(7):371–380 **PMID:** 41565578 460701

Abstract

BACKGROUND: Fibrosis is a pan-organ wound-healing program, yet stromal mechanisms that are liver-selective and connect liver fibrosis to hepatocellular carcinoma (HCC) remain incompletely defined.
METHODS: We assembled public single-cell RNA-seq datasets from fibrotic heart, kidney, liver, and lung with matched controls and applied a unified Seurat integration workflow, differential expression and pathway enrichment, Slingshot pseudotime, and CellChat ligand–receptor inference. We used cross-organ subtraction of shared pan-fibrotic signatures to nominate liver-enriched fibroblast (FB) genes and pathways, intersected these candidates with HCC single-cell datasets and FB trajectories to prioritize fibrosis-aligned, tumor-progression genes, and compared intercellular communication across organs focusing on hepatocyte–FB pairs.
RESULTS: Integration recovered robust FB clusters in each organ without dominant batch effects, supported by canonical FB markers (PDGFRA, LAMB1). Liver FB programs showed endocrine–metabolic rewiring (e.g., insulin/glucagon/FOXO signaling) alongside suppression of xenobiotic/GPCR modules. In HCC, FB subclustering resolved healthy and pathogenic FB states, and Slingshot captured a continuous healthy-to-pathogenic activation axis. Differential expression identified 126 liver-specific upregulated and 239 downregulated DEGs; overlap with HCC pseudotime highlighted SULF2/TIMP3 (fibrosis ↑, progression ↑) and TNFAIP8 (fibrosis ↓, progression ↓). Cross-organ CellChat comparisons further prioritized HGF–MET and AGT–AGTR1B as liver-selective axes relative to heart, kidney, and lung, with stellate-to-hepatocyte (HGF–MET) and hepatocyte-to-stellate (AGT–AGTR1B) ligand–receptor expression correlations observed in liver fibrosis and replicated in independent HCC datasets.

CONCLUSIONS: Cross-organ single-cell integration prioritizes liver-selective stromal circuitry and nominates hepatocyte–FB axes (HGF–MET, AGT–AGTR1B) as plausible links between fibrogenic remodeling and a pro-tumorigenic niche, yielding testable hypotheses at the interface of regeneration, RAS biology, and tumor initiation.

INTRODUCTION

Fibrosis is a maladaptive wound-healing program that culminates in cirrhosis and is tightly linked to hepatocellular carcinoma (HCC). In the liver, quiescent vitamin-A–storing hepatic stellate cells (HSCs) transdifferentiate into proliferative, contractile, collagen-producing myofibroblasts that synthesize extracellular matrix (ECM) and remodel the microenvironment; HSC activation is a central driver of human and experimental liver fibrosis (Tsuchida & Friedman, 2017; Higashi *et al.* 2017; Kamm & McCommis, 2022).

Single-cell transcriptomics has resolved the cellular architecture of cirrhotic livers, identifying scar-associated macrophages and endothelial cells together with PDGFRα$^+$ collagen-producing mesenchyme that engage pro-fibrogenic signaling circuits and nominate actionable targets within the fibrotic niche (Ramachandran *et al.* 2019, Payen *et al.* 2021). Clinically, within the MAFLD/MASLD spectrum, metabolic dysfunction–associated steatohepatitis (MASH) confers elevated HCC risk, and across cohorts fibrosis stage consistently emerges as the dominant predictor of liver-related outcomes and malignant transformation—motivating cross-organ single-cell integration to subtract shared inflammation–ECM–mechanotransduction signatures and isolate liver-specific fibroblast (FB/HSC) programs with oncologic relevance (Ekstedt *et al.* 2015; Dulai *et al.* 2017; Ng *et al.* 2023; Phoolchund *et al.* 2024; Ghazanfar *et al.* 2024).

Building on these advances, this study integrated single-cell datasets from fibrotic heart, liver, kidney, and lung, subtracted pan-organ injury programs, and isolated liver-specific FB differentially expressed genes and pathways that overlap with HCC cohorts. We then quantified intercellular communication using CellChat to identify hepatocyte–FB axes selectively reinforced in liver fibrosis, thereby linking liver-specific stromal remodeling to a pro-tumorigenic niche.

MATERIALS AND METHOD

Dataset Collection

Here, we collected nine public single-cell RNA sequencing datasets comprising liver, heart, kidney, and lung fibrosis samples. Each organ dataset included both fibrosis cases and healthy controls. Details for each dataset including organ, GEO accession, number of cells, and sample counts are provided in Table 1.

Analysis of single cell RNA sequencing data

The Seurat V4 data integration pipeline was used to batch correct the data through the canonical correlation analysis (CCA) method. According to a benchmark comparison study conducted by Tran and colleagues (Tran *et al.* 2020), Seurat CCA was identified as one of the top three preferred batch integration techniques for this type of data. The R package SCTransform (Hafemeister & Satija, 2019) was used to normalize gene expression for each cell by fitting the Gamma-Poisson generalized linear model. The resulting log-transformed, normalized single-cell expression values were used for visualizations and differential expression tests. Statistically significant principal components were determined by a resampling test and were retained for the Uniform Manifold Approximation and Projection (UMAP) analysis. Differential expression analysis among clusters was conducted using a likelihood-ratio test, comparing cells within each cluster against all other cells. Gene A was defined as a biomarker for cluster X if it was detected in at least 25% of cells, had an adjusted *p*-value less than 0.05, and had a log e fold change of at least 0.25 between cells of cluster X and all other cells. These analyses were performed using the Seurat package v4.0. DEGs were analyzed for GO terms and KEGG pathways enrichment by using KOBAS (Bu *et al.* 2021). A significance

Tab. 1. Information of Datasets included

Organ	GEO ID	Number of cells	Number of Samples
Heart	GSE183852	269,794	DCM = 19, Control = 36
Kidney	GSE195460 GSE211785	202,798	DKD = 13, Control = 28
Lung	GSE135893	79,320	IPF = 12, Control = 10
Liver	GSE202379	54,202	NAFLD End Stage = 5, NASH with cirrhosis = 4, NAFLD = 7, Control = 4
Liver	GSE124395 GSE136103 GSE98638 GSE125449	39,470	HCC = 3, NASH = 9, Control = 7

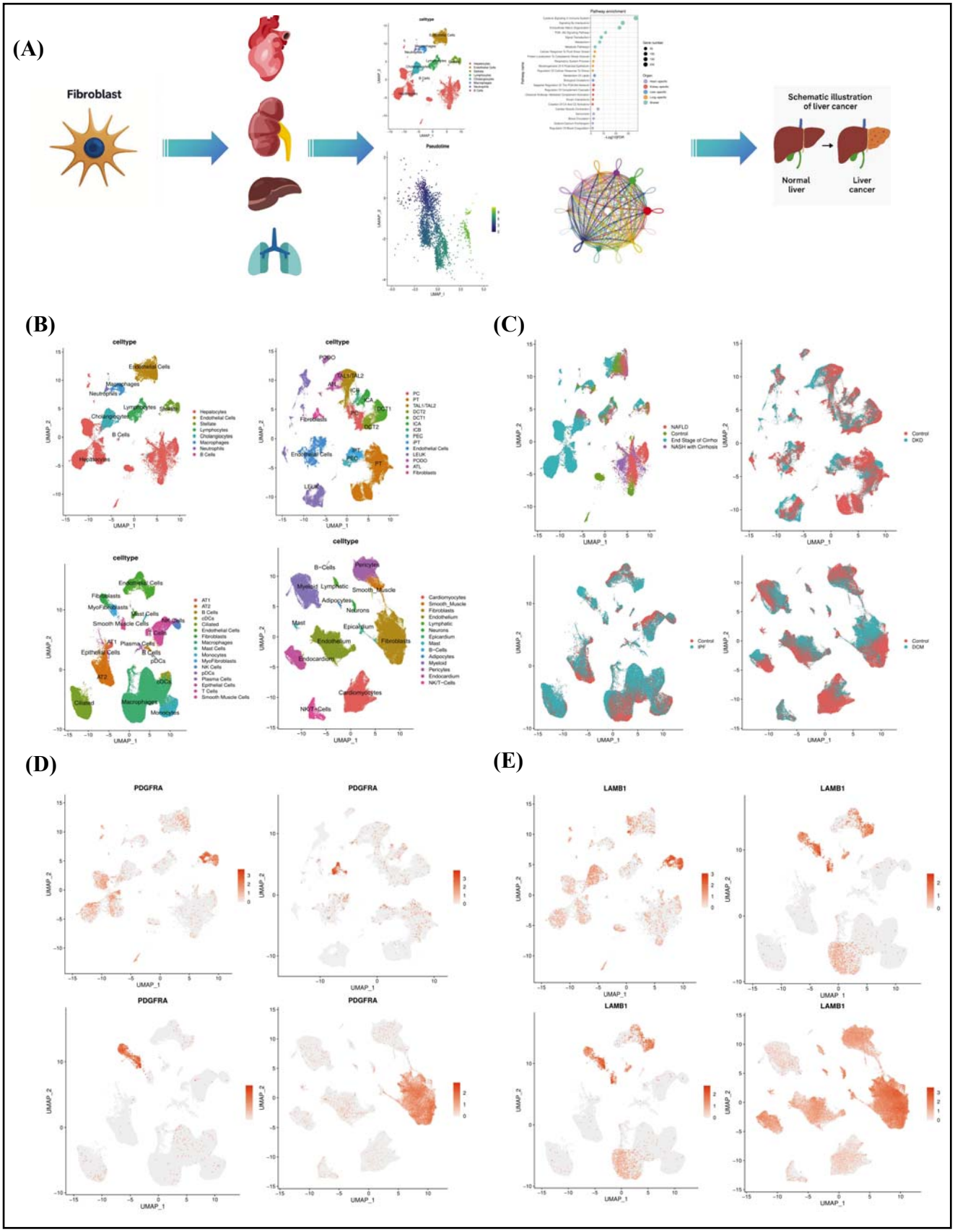

Fig. 1. Integration of public datasets and identification of fibroblast (FB) populations.
(A) Overview of the analytical workflow. (B–E) Distribution of major cell types, disease status, and expression patterns of PDGFRA and LAMB1 across organs. **Upper left**: Liver; **Upper right**: Kidney; **Lower left**: Lung; **Lower right**: Heart.

threshold of FDR < 0.05 was used during the enrichment analysis to identify significant results.

Trajectory analysis of pseudotime

Trajectory analysis was performed using the Slingshot algorithm (Street *et al.* 2018) to infer fibroblast lineage progression based on single-cell transcriptomic data. After normalization and dimensionality reduction, fibroblast clusters were extracted and supplied to Slingshot (v2.6.0) with the UMAP embedding as the input space. Slingshot was used to fit simultaneous principal curves describing smooth trajectories toward activated or pathogenic fibroblast states. The inferred pseudotime values for each cell were extracted from the SlingshotDataSet object for downstream analyses.

Cell-Cell interaction analysis

Cell–cell communication analysis was performed using the CellChat R package (Jin *et al.* 2021) to infer and compare intercellular signaling networks between fibrotic and control samples. For each organ-specific dataset (heart, liver, kidney, and lung), we constructed a CellChat object using normalized single-cell expression matrices after Seurat integration and cell-type annotation. The analysis was restricted to genes encoding known ligands, receptors, and their cofactors as curated in the CellChatDB database. Communication probabilities were computed using a mass action model, followed by statistical inference of significant ligand–receptor interactions ($p < 0.05$). Each interaction was assigned to one of several major signaling pathways according to CellChat's functional grouping.

RESULTS

Integration of public datasets and identification of FB cells

In our cross-organ analysis, we assembled single-cell RNA-seq datasets from fibrotic heart, kidney, liver, and lung and implemented a unified preprocessing/normalization workflow to nominate liver-specific stromal programs. After subtracting pan-fibrotic signatures, we identified differentially expressed genes and pathways selectively enriched in liver fibroblasts (FBs) and overlaid these with trajectory results from independent hepatocellular carcinoma (HCC) cohorts to pinpoint FB-linked genes that increase along tumor progression, together with liver-enriched ligand–receptor signals characteristic of fibrosis (Fig. 1A). For each organ, UMAP embeddings and graph-based clustering consistently resolved a discrete FB cluster (Fig. 1B). Sample-wise coloring of the same embeddings demonstrated adequate cross-sample mixing with no dominant batch-driven aggregates, indicating minimal residual batch effects after integration (Fig. 1C). Marker validation further supported the fidelity of FB calling: PDGFRA showed strong, cluster-restricted expression, while the basement-membrane component LAMB1 mapped concordantly to the same stromal compartment, both clearly segregated from epithelial, endothelial, and immune populations (Fig. 1D–E). Collectively, these results establish a robust cross-organ framework that isolates liver-specific FB signatures.

Liver-specific fibroblast programs feature endocrine–metabolic rewiring and xenobiotic/GPCR suppression

We systematically compared differentially expressed genes (DEGs) that were upregulated or downregulated in fibrotic fibroblasts (FBs) across heart, kidney, liver, and lung (Fig. 2A). Pathway-level enrichment analysis revealed organ-restricted fibroblast (FB) programs. Using a unified threshold (FDR < 0.05), we identified pathways that were selectively upregulated or downregulated in individual organs (Fig. 2B–C). To quantify organ specificity at the gene level, we intersected FB DEGs across all fibrotic datasets and nominated liver-selective signatures, yielding 126 liver-specific upregulated genes and 239 liver-specific downregulated genes (Venn diagrams; Fig. 2D–E); complete gene lists are provided in Table S1. Enrichment analysis of the liver-specific upregulated set was dominated by Glucagon signaling, Insulin signaling, and FOXO-mediated transcription (FDR < 0.05; Fig. 2B), consistent with a liver-centric endocrine–metabolic rewiring of the stromal compartment in fibrosis. In contrast, liver-specific downregulated pathways included Phase I—Functionalization of Compounds (xenobiotic/drug metabolism) and G alpha (i) signaling events (FDR < 0.05; Fig. 2C), indicating attenuation of xenobiotic biotransformation modules and reduced Gi-coupled GPCR inhibitory signaling in fibrotic liver FBs. Notably, under identical selection criteria, the liver FB signatures showed no overlap with the corresponding heart/kidney/lung FB signatures (Fig. 2D–E), supporting their organ-restricted nature. Representative liver-specific FB markers are illustrated in Fig. 2G–I, where ADAMTS13 and NR1H4 (FXR) **displayed** fibrosis-associated decreases, whereas RAPGEF5 **exhibited** a fibrosis-associated increase, reinforcing a model of microvascular/coagulation and bile-acid nuclear-receptor axis attenuation alongside heightened integrin/Rap-driven adhesion signaling in liver fibrosis.

Healthy-to-pathogenic fibroblast transition links fibrosis signatures to HCC

To interrogate whether liver fibrosis–specific fibroblast (FB) signatures are linked to hepatocellular carcinoma (HCC) progression, we assembled public HCC single-cell datasets, identified the FB compartment by canonical stromal markers and graph clustering (Fig. 3A), and harmonized samples to remove batch effects (Fig. 3B). Subclustering of the FB compartment resolved two reproducible states—healthy FB and pathogenic FB—within HCC tissues (Fig. 3C). Marker validation

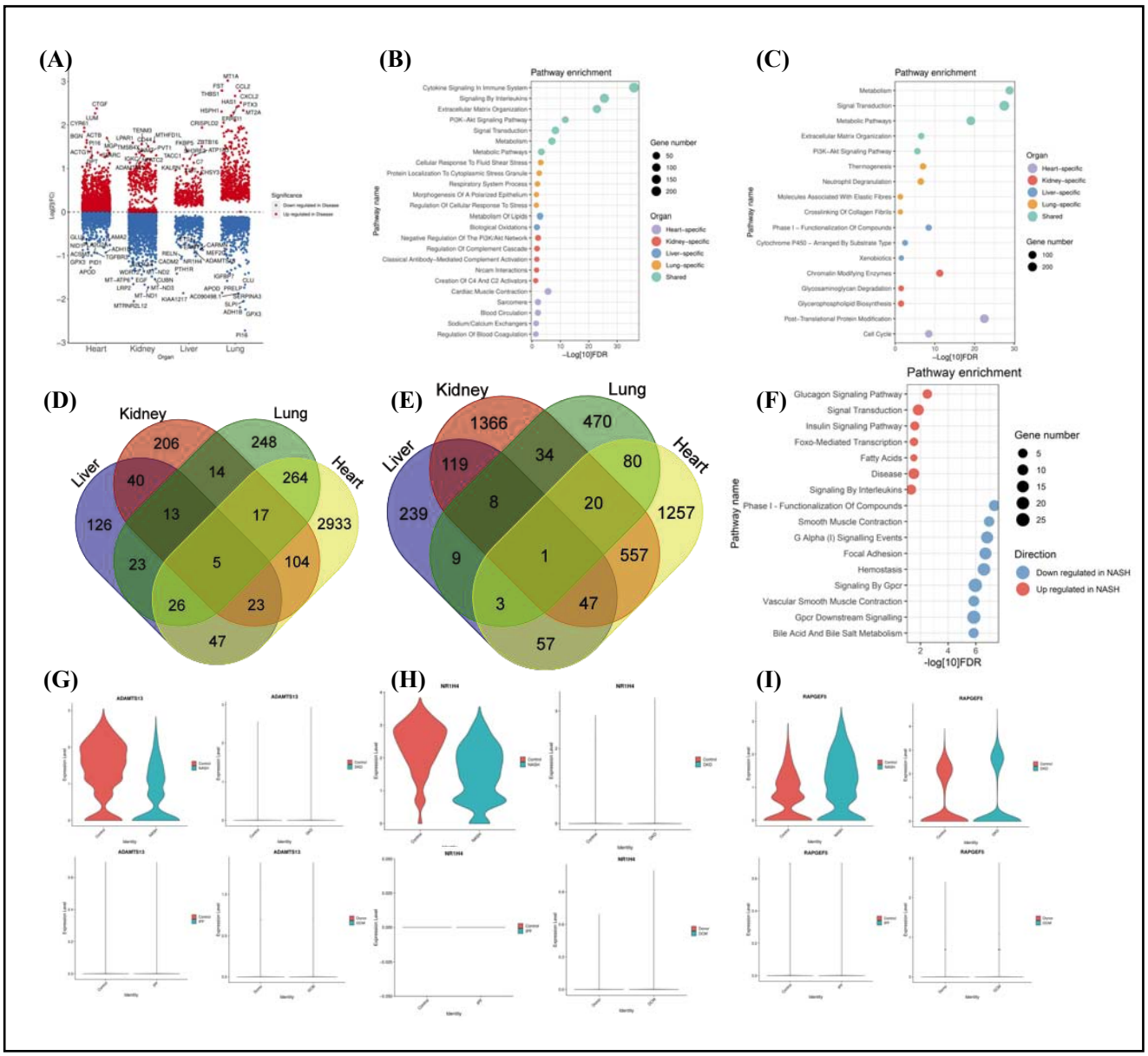

Fig. 2. Liver-specific fibroblast programs exhibit endocrine–metabolic rewiring and suppression of xenobiotic/GPCR signaling.

(A) Dot plot showing statistical comparisons between fibrosis and control groups across organs. x-axis: organ; y-axis: $-\log_2$(fold change).

(B) Bar charts ranking organ-specific upregulated pathways in fibroblasts from fibrotic samples.

(C) Bar charts ranking organ-specific downregulated pathways in fibroblasts from fibrotic samples.

(D) Venn diagram showing overlap of upregulated DEGs among fibrotic fibroblasts across organs.

(E) Venn diagram showing overlap of downregulated DEGs among fibrotic fibroblasts across organs.

(F) Enrichment analyses of liver-specific fibrosis-associated DEGs.

(G, H, I) Violin plots displaying representative liver-specific DEGs across organs. **Upper left**: Liver; **Upper right**: Kidney; **Lower left**: Lung; **Lower right**: Heart.

supported the annotation: COL3A1 (fibrotic collagen I/III program), PDGFRB (activated/perivascular fibroblast receptor), and ACTA2 (αSMA; myofibroblast contractility) localized selectively to the pathogenic FB state, whereas their expression was low or absent in healthy FBs (Fig. 3D–F). Trajectory inference on FBs delineated a continuous pseudotime axis from healthy to pathogenic FBs, indicating a unidirectional activation transition within the tumor microenvironment (Fig. 3G). We then overlapped genes significantly correlated with pseudotime with the liver-fibrosis differentially expressed gene (DEG) sets defined in our cross-organ analysis. Among positively correlated / fibrosis-upregulated genes, two robust overlaps emerged (Fig. 3H): SULF2—an extracellular heparan-sulfate 6-O-endosulfatase that potentiates TGF-β/Wnt/VEGF availability (Fig. 3J)—and TIMP3, a membrane-bound metalloproteinase inhibitor that restrains ADAM17/TACE sheddase activity (Fig. 3K). Conversely, among negatively correlated / fibrosis-downregulated genes,

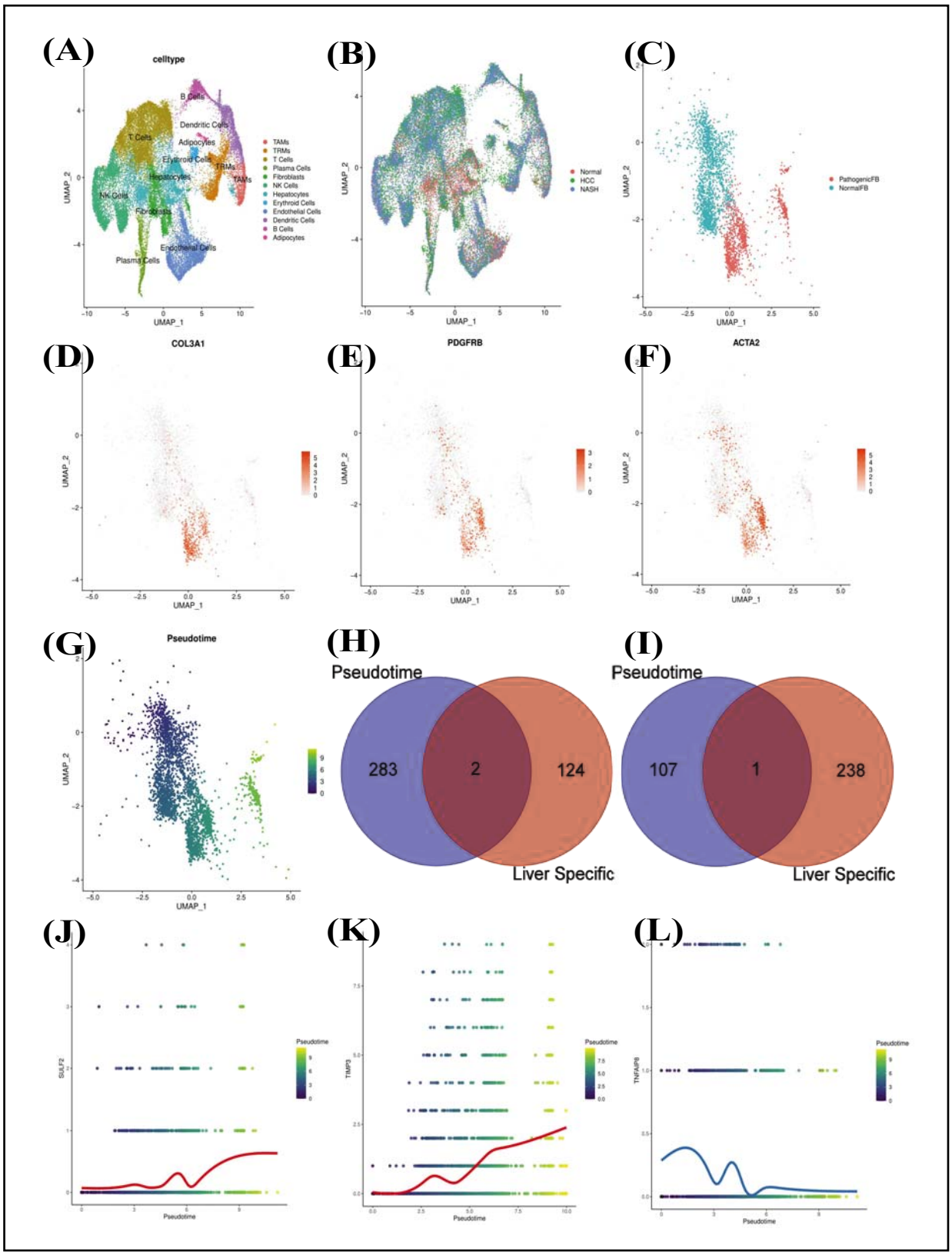

Fig. 3. Transition from healthy to pathogenic fibroblasts links fibrotic signatures to HCC progression.
(A–B) Distribution of major cell types and disease status in HCC datasets.
(C) Composition of fibroblast (FB) subtypes.
(D–F) Expression patterns of pathogenic FB markers (COL3A1, PDGFRB, ACTA2).
(G) Pseudotime trajectory depicting the transition from normal to pathogenic FBs.
(H) Venn diagrams illustrating the overlap of positively correlated and upregulated DEGs shared between HCC and liver fibrosis datasets.
(I) Venn diagrams illustrating the overlap of negatively correlated and downregulated DEGs shared between HCC and liver fibrosis datasets.
(J–L) Regression analyses showing the relationship between SULF2, TIMP3, and TNFAIP8 expression levels and pseudotime progression.

we identified a single overlap (Fig. 3I): TNFAIP8, a TIPE-family regulator implicated in inflammatory homeostasis (Fig. 3L). Collectively, these results establish that the liver-specific fibrotic FB program captured in non-malignant fibrosis converges with the healthy to pathogenic FB transition within HCC, nominating SULF2 and TIMP3 as reinforced pro-fibrotic axes and TNFAIP8 as a diminished anti-inflammatory node during tumor-associated stromal remodeling.

Liver fibrosis–specific communication axes converge on HGF–MET and AGT–AGTR1B

Across public single-cell fibrosis datasets from heart, liver, kidney, and lung, we inferred intercellular communication and visualized pathway activity per cell type using heatmaps (Fig. 4A–H). Representative pathways recapitulated known biology (e.g., robust VEGF signaling in endothelial cells), supporting the validity of the approach. Comparative analysis across the four organs progressively narrowed the liver-specific signal to AGT (renin–angiotensin) and HGF pathways: relative to the other organs, liver fibrosis showed selective enrichment of these axes, whereas matched healthy controls lacked such reinforcement (liver fibrosis/control: Fig. 4A-B; kidney fibrosis/control: Fig. 4C–D; lung fibrosis/control: Fig. 4E–F; heart fibrosis/control: Fig. 4G–H). Focusing on ligand–receptor pairs, we detected stellate to hepatocyte HGF to MET and hepatocyte to stellate AGT to AGTR1B interactions (Fig. 4I–J), both of which were independently validated in an external HCC dataset (Fig. 4K–L). Consistent with these network-level findings, expression maps confirmed upregulation of HGF and AGT within their respective source cell populations in liver fibrosis (Fig. 4M–P), suggesting that these paired signals may facilitate the stromal–parenchymal coupling that promotes progression from liver fibrosis toward hepatocarcinogenesis.

DISCUSSION

Using cross-organ single-cell integration with explicit subtraction of pan-fibrotic injury programs, we isolated liver-selective fibroblast (FB) features that may connect fibrogenic remodeling to hepatocarcinogenesis. Specifically, liver FBs exhibited an endocrine–metabolic rewiring dominated by Glucagon/Insulin/FOXO signaling (upregulated), and cell–cell communication inference prioritized HGF–MET and AGT–AGTR1B as liver-enriched hepatocyte–FB axes that were not detected in the corresponding heart/kidney/lung FB signatures under the same criteria. Linking non-malignant fibrosis to independent HCC cohorts further highlighted concordant nodes—SULF2/TIMP3 (fibrosis ↑, progression ↑) and TNFAIP8 (fibrosis ↓, progression ↓)—supporting persistence of these liver-selective programs into the HCC tumor microenvironment. This cross-organ comparator framework helps mitigate a common limitation of organ-restricted studies (i.e., conflating shared injury responses with organ-specific mechanisms) while refining and extending foundational concepts of hepatic stellate cell activation in fibrogenesis and recent single-cell atlases of stromal heterogeneity (Kamm & McCommis, 2022; Ramachandran *et al.* 2019).

Clinically, fibrosis stage is a dominant predictor of adverse outcomes across NAFLD/MASLD and is tightly linked to hepatocarcinogenesis (replace citations with short author–year format). Our trajectory analyses indicated that the healthy-to-pathogenic FB continuum observed in HCC mirrored liver-fibrosis programs, providing a mechanistic bridge between stromal remodeling in chronic liver disease and pro-tumorigenic niche evolution. In particular, we identified SULF2 and TIMP3 as fibrosis-upregulated, pseudotime-positive nodes and TNFAIP8 as a fibrosis-downregulated, pseudotime-negative node—features consistent with an extracellular milieu that (i) increases growth-factor bioavailability via heparan sulfate editing, (ii) alters protease/inhibitor balance linked to cytokine/EGFR-ligand shedding, and (iii) relaxes immune homeostatic constraints. While causal roles require perturbational testing, these patterns map naturally onto established HSC biology (ECM deposition, contractility, cytokine signaling) (Tsuchida & Friedman, 2017; Higashi *et al.* 2017; Matsumoto & Nakamura, 2014) and stromal circuits highlighted by single-cell atlases (Kamm & McCommis, 2022; Ramachandran *et al.* 2019).

A central insight from our cell–cell communication analysis is the selective reinforcement of HGF–MET and AGT–AGTR1B in liver fibrosis relative to other organs. HGF–MET is a canonical hepatotropic axis governing hepatocyte survival, proliferation, and regeneration; genetic and pharmacologic perturbations modulate liver repair and fibrosis (Ghazanfar *et al.* 2024; Zhao *et al.* 2022; Nakamura *et al.* 2011; Matsumoto & Nakamura, 1992). Its stellate-to-hepatocyte reinforcement in fibrosis and recurrence in HCC is consistent with a regeneration–fibrosis coupling model, whereby regenerative signaling within a matrix-rich niche can be co-opted to favor oncogenic progression. The renin–angiotensin system (RAS) signal we observe—hepatocyte-derived AGT engaging stellate-cell AGTR1B (AT1)—is especially plausible in the liver, a principal source of circulating angiotensinogen (Matsusaka *et al.* 2012). Extensive preclinical evidence supports that AngII/AT1 signaling promotes HSC proliferation, TGF-β induction, contractility, and collagen production, while RAS blockade or activation of the ACE2/Ang-(1–7)/Mas counter-axis is anti-fibrotic (Yoshiji *et al.* 2001; Wei *et al.* 2000; e Silva & Silveira, 2013; Murphy *et al.* 2015). Together, these hepatocyte–FB axes plausibly couple fibrogenic remodeling to regenerative and microenvironmental rewiring, creating conditions permissive for malignant transformation.

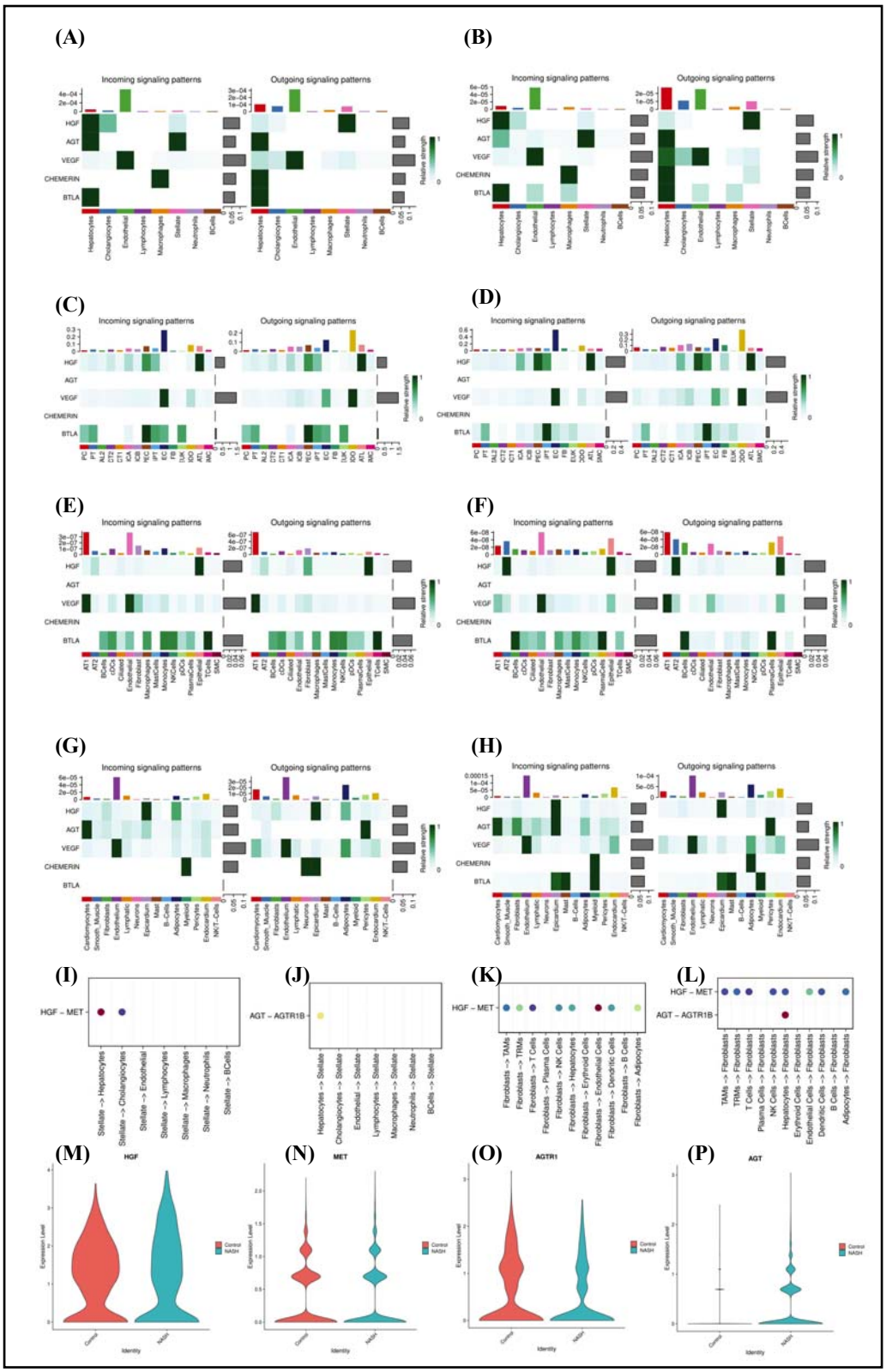

Fig. 4. Liver fibrosis–specific communication networks converge on the HGF–MET and AGT–AGTR1B signaling axes.
(A–H) Heatmaps showing pathway activities derived from cell–cell interaction analyses. Liver fibrosis/control: (A–B); kidney fibrosis/control: (C–D); lung fibrosis/control: (E–F); heart fibrosis/control: (G–H).
(I, K) Dot plots highlighting ligand–receptor gene pairs identified between hepatic stellate cells and other cell types within the HGF and AGT signaling pathways in liver fibrosis and HCC datasets.
(J, L) Dot plots highlighting ligand–receptor gene pairs identified from other cell types to hepatic stellate cells in the same pathways.
(M, O) Violin plots showing the expression levels of HGF and AGTR1B (human ortholog: AGTR1) in stellate (fibroblast) populations.
(N, P) Violin plots showing the expression levels of MET and AGT in hepatocyte populations.

Nevertheless, several limitations remain. First, cross-organ subtraction is limited by severity mismatches in our cohort assembly (Table 1): the liver dataset is enriched for "End Stage" and "Cirrhosis" samples, whereas heart and kidney datasets capture broader disease spectrums and potentially earlier stages. Consequently, some signals classified as "liver-selective" may partially reflect advanced-stage/decompensation remodeling rather than purely organ-intrinsic biology, and we interpret our prioritized targets as most directly relevant to advanced liver disease. Second, pseudotime is an inferred surrogate for progression; complementary spatial transcriptomics and lineage/temporal readouts will be essential to verify physical apposition and directionality along the HGF/AGT axes. Third, while overlap with HCC trajectories supports cross-context consistency, mechanistic testing—e.g., perturbation of HGF–MET and/or AGT–AGTR1B, and modulation of fibrosis-aligned nodes such as SULF2/TIMP3, in primary human stellate cells and precision-cut liver slices—will be required to assess whether multi-node targeting can blunt pathogenic FB transitions and downstream niche remodeling.

In sum, cross-organ single-cell integration that subtracts shared injury programs prioritizes liver-selective fibroblast circuitry and nominates two hepatocyte–FB axes—HGF–MET and AGT–AGTR1B—as plausible links between liver fibrosis and HCC risk. Rather than broadly stating "actionable entry points" we frame testable predictions: in precision-cut liver slices, perturbation of HGF–MET and/or AGT–AGTR1B signaling, alone or in combination with modulation of fibrosis-aligned nodes such as SULF2/TIMP3, should shift the liver-FB program away from a fibrosis-to-HCC trajectory. In parallel, the liver-FB Glucagon/FOXO endocrine–metabolic signature represents a candidate biomarker readout to monitor pathway engagement and progression in advanced MASLD/MASH and early HCC.

CONFLICT OF INTEREST

The authors declare that the research was conducted in the absence of any commercial or financial relationships that could be construed as a potential conflict of interest.

AUTHOR CONTRIBUTIONS

Conceptualization, Shuna Zhang; Data curation Shuna Zhang; Formal analysis, Shuna Zhang; Funding acquisition, Xin Li; Investigation, Pei Sun; Methodology, Shuna Zhang; Project administration, Xin Li; Resources, Jian Zhang; Software, Shuna Zhang; Supervision, Xin Li; Validation, Shuna Zhang; Visualization, Shuna Zhang; Writing - original draft, Shuna Zhang; Writing – review & editing, Shuna Zhang, Pei Sun, Jian Zhang and Xin Li.

FUNDING

This work was supported by Capital's Funds for Health Improvement and Research (2024-1-1203); Dengfeng Talent Support Program of Beijing Municipal Administration of Hospitals (No.DFL20221601); High-level Public Health Technical Personnel Construction Project (Subject leaders-03-21).

ACKNOWLEDGMENTS

Not applicable.

REFERENCES

1 Bu D, Luo H, Huo P, Wang Z, Zhang S, He Z et al. (2021). KOBAS-i: intelligent prioritization and exploratory visualization of biological functions for gene enrichment analysis. Nucleic Acids Res. **49**(W1): W317–W325. doi: 10.1093/nar/gkab447
2 Higashi T, Friedman SL, Hoshida Y (2017). Hepatic stellate cells as key target in liver fibrosis. Adv Drug Deliv Rev. **121**: 27–42. doi: 10.1016/j.addr.2017.05.007
3 Dulai PS, Singh S, Patel J, Soni M, Alberino D, Kachadoorian M et al. (2017). Increased risk of mortality by fibrosis stage in nonalcoholic fatty liver disease: Systematic review and meta-analysis. Hepatology. **65**(5): 1557–1565. doi: 10.1002/hep.29085
4 e Silva ACS, Silveira KD, Ferreira AJ, Teixeira MM (2013). ACE2/Ang-(1-7)/Mas axis in inflammation and fibrosis. Curr Opin Nephrol Hypertens. **22**(2): 153–160. doi: 10.1097/MNH.0b013e32835b8e9e
5 Ekstedt M, Hagström H, Nasr P, Fredrikson M, Stål P, Kechagias S et al. (2015). Fibrosis stage is the strongest predictor for disease-specific mortality in NAFLD after up to 33 years of follow-up. Hepatology. **61**(5): 1547–1554. doi: 10.1002/hep.27368
6 Ghazanfar H, O'Neill S, Lucocq J, Bateman A, Palmer CNA, Gribbin H et al. (2024). Metabolic dysfunction-associated steatohepatitis and HCC. Nutrients. **16**(7): 1103. doi: 10.3390/nu16071103
7 Hafemeister C, Satija R (2019). Normalization and variance stabilization of single-cell RNA-seq data using regularized negative binomial regression. Genome Biol. **20**(1): 296. doi: 10.1186/s13059-019-1874-1
8 Jin S, Guerrero-Juarez CF, Zhang L, Chang I, Ramos R, Kuan CH et al. (2021). Inference and analysis of cell-cell communication using CellChat. Nat Commun. **12**(1): 1088. doi: 10.1038/s41467-021-21246-9
9 Kamm DR, McCommis KS (2022). Hepatic stellate cells in physiology and pathology. J Physiol. **600**(9): 1825–1837. doi: 10.1113/JP282207
10 Matsumoto K, Nakamura T (1992). Hepatocyte growth factor: roles in liver regeneration. J Gastroenterol Hepatol. **7**(5): 452–459. doi: 10.1111/j.1440-1746.1992.tb01022.x
11 Matsumoto K, Nakamura T (2014). HGF/c-Met in regeneration and drug discovery. Biomedicines. **2**(4): 275–300. doi: 10.3390/biomedicines2040275
12 Matsusaka T, Niimura F, Shimizu A, Pastan I, Saito A, Kobori H et al. (2012). Liver-derived angiotensinogen is the primary source of renal angiotensin II. J Clin Invest. **122**(8): 2963–2976. doi: 10.1172/JCI62661
13 Murphy AM, Joy L, Molinaro G, Carter C, Stewart DJ, Cianflone K (2015). Angiotensin-(1-7) axis reduces HSC activation and fibrosis (review). Ann Transl Med. **3**(18): 266. doi: 10.3978/j.issn.2305-5839.2015.10.11
14 Nakamura T, Sakai K, Nakamura T (2011). Discovery and biology of HGF. Cytokine Growth Factor Rev. **21**(4): 299–307. doi: 10.1016/j.cytogfr.2010.07.001
15 Ng CH, Tan DJH, Lim WH, Lim SY, Tan XX, Lim TY et al. (2023). Mortality Outcomes by Fibrosis Stage in Nonalcoholic Fatty Liver Disease: A Systematic Review and Meta-analysis. Clin Gastroenterol Hepatol. **21**(4): 980–993.e11. doi: 10.1016/j.cgh.2022.05.013

16 Payen VL, Silvério N, Hamad O, Toussaint F, Humblin F, Urbain D et al. (2021). Single-cell RNA sequencing of human liver reveals hepatic stellate cell heterogeneity. Hepatol Commun. **5**(8): 1372–1388. doi: 10.1002/hep4.1752
17 Phoolchund AGS, Vispoel M, Tabbaa S, Hansen A, Hyder O (2024). MASLD and the Development of HCC: Pathogenesis and Therapeutic Challenges. Hepatoma Res. **10**: 31. doi: 10.20517/hepres.2024.23
18 Ramachandran P, Dobie R, Wilson-Kanamori JR, Dora SK, Henderson BE, Lu Y et al. (2019). Resolving the fibrotic niche of human liver cirrhosis at a single-cell level. Nature. **575**(7783): 512–518. doi: 10.1038/s41586-019-1631-3
19 Street K, Risso D, Fletcher RB, Das D, Ngai J, Yosef N et al. (2018). Slingshot: cell lineage and pseudotime inference for single-cell transcriptomics. BMC Genomics. **19**(1): 477. doi: 10.1186/s12864-018-4772-0
20 Tran HTN, Ang KS, Chevrier M, Zhang X, Lee NYS, Goh M et al. (2020). A benchmark of batch-effect correction methods for single-cell RNA sequencing data. Genome Biol. **21**(1): 12. doi: 10.1186/s13059-019-1850-9
21 Tsuchida T, Friedman SL (2017). Mechanisms of hepatic stellate cell activation. Nat Rev Gastroenterol Hepatol. **14**(7): 397–411. doi: 10.1038/nrgastro.2017.38
22 Wei HS, Li DG, Lu HM, Zhao L, Zhang MS, Guo LH et al. (2000). ACE inhibitors and AT1 blockade ameliorate CCl4-induced hepatic fibrosis. World J Gastroenterol. **6**(6): 815–820. doi: 10.3748/wjg.v6.i6.815
23 Yoshiji H, Kuriyama S, Yoshii J, Ikenaka Y, Noguchi R, Hicklin DJ et al. (2001). Angiotensin II type 1 receptor interaction drives HSC proliferation and TGF-beta up-regulation. J Hepatol. **35**(3): 316–323. doi: 10.1016/s0168-8278(01)00133-1
24 Zhao Y, Zhang Y, Liu Y, Wang S, Wang Q, Li H et al. (2022). HGF/c-Met: a key promoter in liver regeneration. Int J Mol Sci. **23**(7): 3741. doi: 10.3390/ijms23073741.